

Appendix

Estimating underwater light regime under spatially heterogeneous sea ice in the Arctic

Contents

Smoothing radiance data	3
Raman inelastic scattering	6
HydroLight simulations	6

List of Figures

1	The field campaign was part of the GreenEdge project (www.greenedgeproject.info) which was conducted on landfast ice southeast of the Qikiqtarjuaq Island in the Baffin Bay (67.4797N, 63.7895W).	2
2	Examples showing the number of downward irradiance (A) and upward radiance (B) photons captured by the software detectors at different depth ranges (numbers in gray boxes) as a function of the distance from the melt pond. The red lines represent the fitted Gaussian curves.	3
3	Scatter plots showing the relationships between downward irradiance ($E_d(z)$) and upward radiance ($L_u(z)$) between 400 and 700 nm at different depths (numbers in gray boxes). Red lines represent the regression lines of the fitted linear models. Dashed lines are the 1:1 lines. Note the high dispersion occurring in the orange and red regions (≥ 600 nm).	4
4	Average determination coefficients R^2 and standard deviation (shaded area) of the regressions between normalized (at 10 meters) $E_d(z)$ and $L_u(z)$ profiles between 400 and 700 nm. At each wavelength, average values were computed from the 83 COPS measurements. A sharp decrease of R^2 occurred after approximately 575 nm, suggesting a gradual decoupling between $E_d(z)$ and $L_u(z)$ profiles at longer wavelengths, possibly due to the effect of inelastic scattering.	5
5	Scatter plots showing the relationships between K_d and K_{Lu} calculated from the downward irradiance and upward radiance profiles modelled with and without including Raman scattering. The dashed lines represent the 1:1 lines.	7



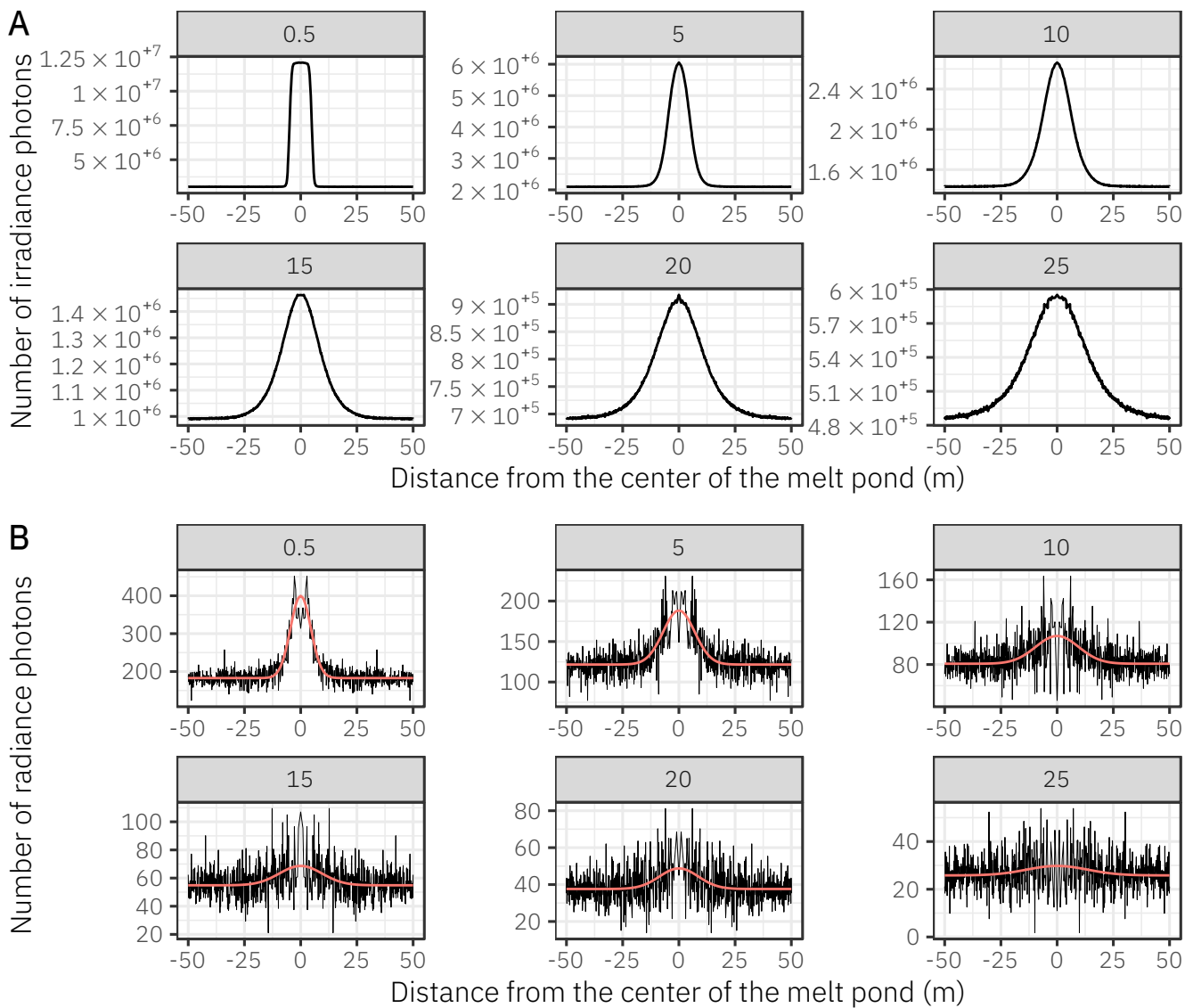
Supplementary Fig. 1: The field campaign was part of the GreenEdge project (www.greenedgeproject.info) which was conducted on landfast ice south-east of the Qikiqtarjuaq Island in the Baffin Bay (67.4797N, 63.7895W).

Smoothing radiance data

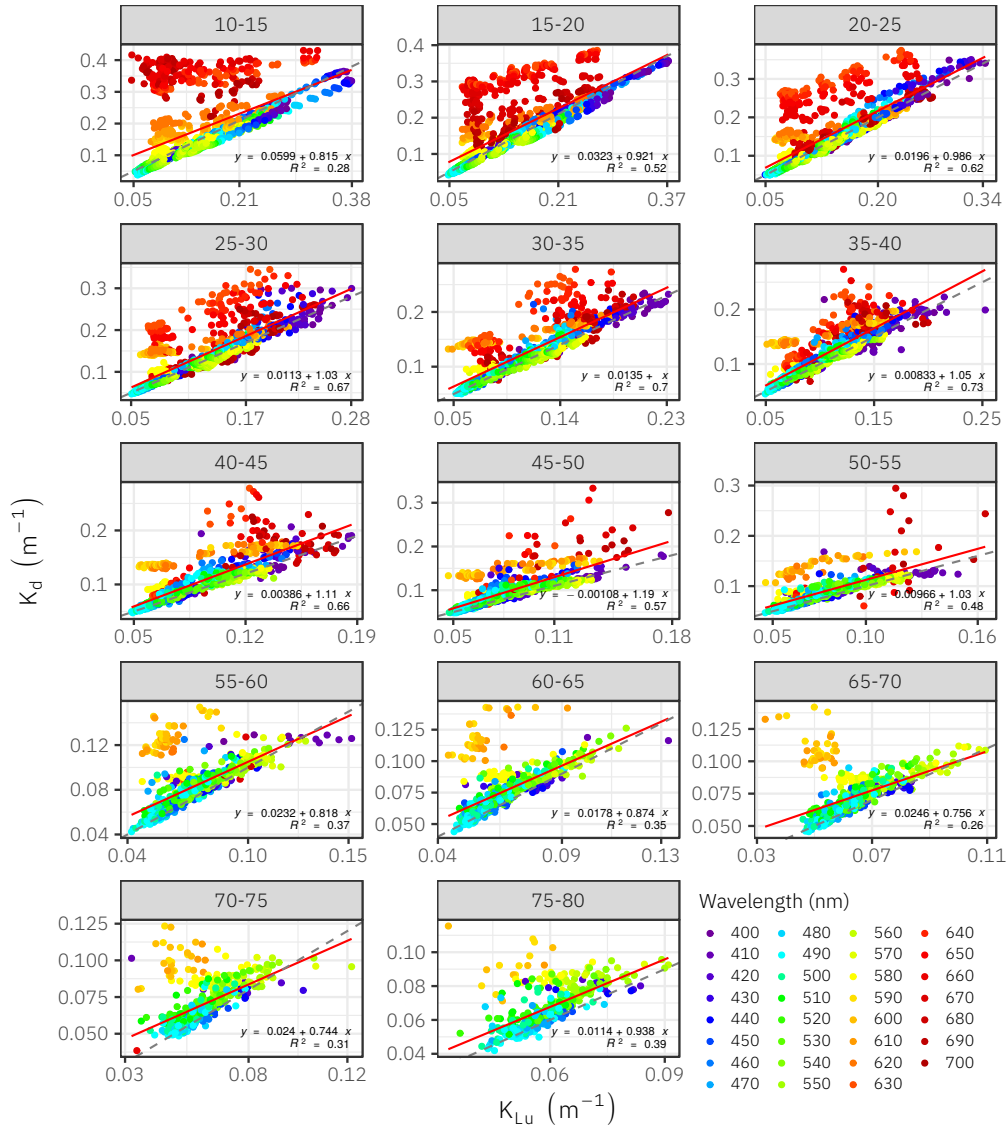
Due to the low scattering coefficients used to reproduce in situ conditions observed during the sampling campaign, radiance profiles were noisy because only few photons were scattered back in the upward direction (note the different y-scales). To overcome this problem, upward radiance data were smoothed using Gaussian fittings according to equation 1:

$$f(x, \varphi, \mu, \sigma, k) = \varphi e^{-\frac{(x - \mu)^2}{2\sigma^2}} + k \quad (1)$$

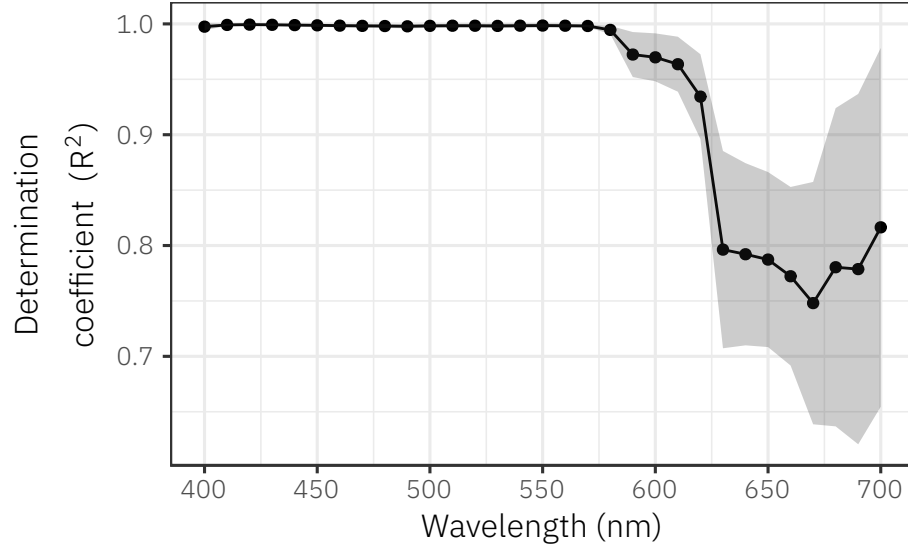
where x (m) is the horizontal distance from the center of the melt pond, σ (m) is the standard deviation controlling the width of the curve, φ is the height of the curve peak ($\varphi = \frac{1}{\sigma\sqrt{2\pi}}$), μ (m) is the position of the center of the peak and k an offset coefficient.



Supplementary Fig. 2: Examples showing the number of downward irradiance (A) and upward radiance (B) photons captured by the software detectors at different depth ranges (numbers in gray boxes) as a function of the distance from the melt pond. The red lines represent the fitted Gaussian curves.



Supplementary Fig. 3: Scatter plots showing the relationships between downward irradiance ($E_d(z)$) and upward radiance ($L_u(z)$) between 400 and 700 nm at different depths (numbers in gray boxes). Red lines represent the regression lines of the fitted linear models. Dashed lines are the 1:1 lines. Note the high dispersion occurring in the orange and red regions (≥ 600 nm).



Supplementary Fig. 4: Average determination coefficients R^2 and standard deviation (shaded area) of the regressions between normalized (at 10 meters) $E_d(z)$ and $L_u(z)$ profiles between 400 and 700 nm. At each wavelength, average values were computed from the 83 COPS measurements. A sharp decrease of R^2 occurred after approximately 575 nm, suggesting a gradual decoupling between $E_d(z)$ and $L_u(z)$ profiles at longer wavelengths, possibly due to the effect of inelastic scattering.

~~Raman inelastic scattering~~

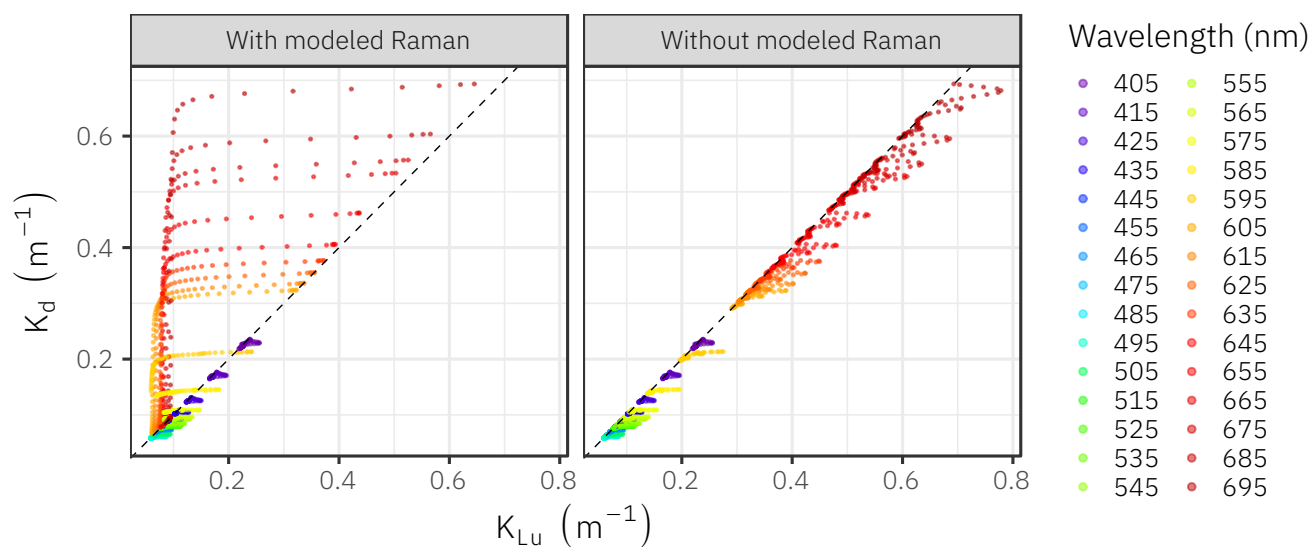
Raman scattering is a process by which photons, interacting with water molecules, lose or gain energy and are scattered at a different wavelength than the one they were originating from. In Supplementary Fig. 3 and Supplementary Fig. 4, one can observe a decoupling between K_d and K_{Lu} at longer wavelengths, possibly due to inelastic Raman scattering. To validate this hypothesis, we used the HydroLight radiative transfer numerical model to calculate downward irradiance and upward radiance and their associated attenuation coefficients in a water column.

~~HydroLight simulations~~

Two HydroLight simulations were carried out to model downward irradiance and upward radiance with and without taking into account Raman inelastic scattering. The simulations were parameterized using an IOPs profile (ac-s from Sea-Bird Scientific) measured on the first of May 2015 in the Baffin Bay. Simulations were performed with the following characteristics:

- A surface free of ice.
- A surface without waves.
- Sun position at noon for May 1st.
- A cloudless sky.
- No fluorescence.
- Using HydroLight default atmospheric parameters.
- The scattering phase function was described by a Fournier-Forand analytic form with a 3% backscatter fraction.
- EcoLight option was run.

The HydroLight simulations showed a decoupling between K_d and K_{Lu} starting at around 600 nm when Raman scattering was modelled (Supplementary Fig. 5). The same decoupling was also observed with the in situ data (see Supplementary Fig. 3).



Supplementary Fig. 5: Scatter plots showing the relationships between K_d and K_{Lu} calculated from the downward irradiance and upward radiance profiles modelled with and without including Raman scattering. The dashed lines represent the 1:1 lines.